UNIVERSITY OF CALIFORNIA SAN DIEGO

PPC-Striatal Projection Neurons Encode History-Based Behavioral Bias

A Thesis submitted in partial satisfaction of the requirements for the degree Master of Science

in

Biology

by

Trevor Daniel Link

Committee in charge:

Professor Takaki Komiyama, Chair
Professor Byungkook Lim, Co-Chair
Professor Amy Kiger

2018

The Thesis of Trevor Daniel Link is approved, and it is acceptable in quality and form for publication on microfilm and electronically:

Co-Chair

Chair

University of California San Diego

2018

TABLE OF CONTENTS

LIST OF ABBREVIATIONS

AuD- secondary auditory cortex

AUROCC- Area under the ROC curve

CA1- hippocampus

Cg- cingulate cortex

ITI- Inter-trial interval

LoH- Light over Headbar (Control)

LPtA- lateral Parietal association cortex

M1- Primary motor cortex

M2- Secondary motor cortex

Non-Proj- Non-Projection Neurons

Po- -posterior thalamic nuclear group

ROC- Receiver Operating Characteristic

ROI- Region of Interest

RSA- Retrospleniual cortex, agranular

RSG- Retrosplenial cortex, granular

S1BF- somatosensory 1, barrel field

S1DZ- somatosensory 1- dysgranular zone

S1FL- somatosensory 1- forelimb region

S1HL- somatosensory 1- hindlimb region

S1Tr- somatosensory 1- Trunk region

S1Sh-

S2- second somatosensory cortex

STR- Striatum

V1- primary visual cortex

V2L- secondary visual cortex, lateral

V2M- secondary visual cortex, medial

VL- ventrolateral thalamic nucleus

VPL- ventral posterolateral thalamic nucleus

LIST OF FIGURES

LIST OF GRAPHS

ACKNOWLEDGEMENTS

I would like to acknowledge Professor Takaki Komiyama, as the chair of my committee, and whom which this was all possible. He provided the essential support necessary to complete all of the data collection and essential analysis for this project. His guidance and assistance has proven to be invaluable.

I would also like to acknowledge EunJung Hwang, who has been essential for every aspect of this project. She was always available for questions about the project, troubleshooting, methods, analysis, thesis writing and beyond. She always pushed me to think critically about what any why we were running the project in a particular way. Without her this project would not have been possible.

I would like to acknowledge the Shan Lu, who was responsible for teaching me all of the methods that I had used during this project. She gave me the essential techniques to complete the project.

This thesis is in part currently being prepared for submission for publication of the material. Hwang, EunJung; Link, Trevor; Lu, Shan; Komiyama, Takaki. The thesis author was a primary investigator of this material.

ABSTRACT OF THE THESIS

PPC-Striatal Projection Neurons Encode History-Based Behavioral Bias

by

Trevor Daniel Link

Master of Science in Biology

University of California San Diego, 2018

Professor Takaki Komiyama, Chair
Professor Byungkook Lim, Co-Chair

Posterior Parietal Cortex (PPC) has been shown in the past to encode history-based behavioral biases. In this thesis project, we attempted to elucidate the input-output pathways of PPC that are responsible for history-dependent choice bias. We found through the use of retrograde labelling, two-photon calcium imaging, and optogenetic inactivation that the PPC neurons projecting to the striatum (STR) are responsible for the production of this history-dependent bias rather than the neurons projecting to the secondary motor cortex (M2). We also found through monosynaptic rabies-virus tracing that STR-projection neurons receive stronger inputs from association areas such as the cingulate, retrosplenial and secondary visual cortices than M2-projection neurons. Therefore, we propose that history-dependent choice bias is produced as PPC processes information from the associative and sensory cortices and sends the

processed bias information to STR in which the bias is likely integrated with other decision variables such as sensory evidence.

Introduction

When people mention bias, it often has negative connotations associated with it. It normally comes up in conversations about subjects like politics, socioeconomic issues, and cultural debates involving highly charged topics such as race and gender to name a few examples. But it is much more neutral than most people associate with it. People are biased towards their own particular interest with mundane topics like food, music, and travel routes. Bias can also come in the form of particular behaviors, often with specific sequences of repetitive behaviors such as grabbing an item with the dominant hand more often than the non-dominant hand. These biases have had some benefit in the past, such as more nutritious food, faster travel routes, deeper relaxation and so forth.

All these examples are often called free-choices, where there is no correct or incorrect answer to a question (Erlich et al, 2015). Both choices given are equally salient and neither will give a reward or punishment when the choice is made. A region of the brain called the Posterior Parietal Cortex (PPC) has been implicated in the past of the coding of these free-choices. This region has a heterogenous array of neurons with a variety of potential functions (Hwang & Anderson, 2011)(Morcos & Harvey, 2016). It has also been implicated in functions such as the combined encoding of stimulus and choice (Goard et al, 2016) and that it continues its encoding of sensory motor information throughout a task (Harvey et al, 2012).

With the vast majority of choices having some form of reinforcement on behavior, these choices will inevitably impact future behaviors. Hwang et al 2017 showed that they could construct a model to predict the choice of a mouse during a joystick task based on its choice history. The model would utilize the constant τ (Sugrue, 2004) to weigh the most recent trials heaviest in its impact on the next trials behavior, with less recent trials exponentially decaying.

Recent choices have a much larger impact on action than earlier choices do (Parker et al, 2016). They had used a model to predict the behavior of mice individually with 70% certainty given the previous behavioral data from passed trials in the same experimental session. They noticed that during the PPC inactivation trials, the model accuracy had decreased. Interestingly, these results are temporally precise, as this result was only true if they inactivated the PPC during the inter-trial interval (Hwang et al, 2017). If it was on during any other time in the trial, the model could predict with similar accuracy to that of the light being off. This showed that the change in model accuracy was in fact caused by the change in history-dependency, which was producing a choice bias.

Previous research on the PPC has elucidated that it has some function in the integration of sensory information with motor information (Mohan et al, 2018). This region is known for having a variety of inputs from regions such as motor cortices and somatosensory cortex and outputs to the basal ganglia, as well as being a part of the S1-PPC-M1 pathway (Mohan et al, 2018)(Hovde et al, 2018). The PPC is known to be an association area, containing inputs from both sensory areas of the brain as well as motor regions. In particular, the motor areas and the PPC have reciprocal connections not seen in those between the PPC and the somatosensory regions of the brain (Yager et al, 2015).

The Hwang et al paper discovered that neurons within the PPC were encoding choice bias, produced prior to the presentation of a stimulus, and was offloaded to another region of the brain. The question then arose, where was this information going? This was the basis of our project and my thesis, to discern the location or locations the information is being offloaded. Based on prior experiments, two potential locations we investigated the information could be offloaded are the striatum and M2.

The Striatum is known as the major motor hub of the brain, with a large amount of connections from the cortex, being that it is an integral portion of the cortico-basal ganglia-thalamic circuit (Yager et al, 2015). It possesses multiple types of cells, including D1R and D2R MSNs (Yager et al, 2015), cholinergic interneurons (Goldberg & Reynolds, 2011), and GABAergic interneurons (Tepper et al, 2010). Being the largest nucleus in the basal ganglia, the striatum receives a majority of its inputs from the cortex, as well as a large amount of its inputs from other regions, such as the thalamus, hippocampus and inferior temporal gyrus (Stocco et al, 2010).

The dorsal striatum has historically been known to control and integrate motor action (Znamenskiy & Zador, 2013), as well as encoding classical conditioning through stimulus response learning (Yager et al, 2015)(Balleine et al, 2007). One experiment showed selective inactivation of projection cells terminating in the striatum altered behaviors associated with stimulus driven action selection.

The secondary motor area, or M2, is known to be involved in goal directed actions, and is critical for updating behavior based on the consequences of actions (Gremel & Costa, 2013). M2 has an increased level of activity during the initial portions of learning (Nachev et al, 2008). When injected with muscimol, old tasks are unaffected, while the ability to learn new tasks has been inhibited (Nachev et al, 2008).

Either of these locations could be plausible regions the history-dependent choice bias information from PPC could be sent prior to the introduction of the visual stimulus.

Methods

All procedures were in accordance with protocols approved by the University of California, San Diego International Animal Care and Use Committee and guidelines of the National Institute of Health. Animals were housed in cages in a room with reverse light cycling, with the lights timed to 10:00 and 22:00 switches. Experiments were done around the night cycle switches and throughout the night cycle.

Most procedures were adapted from *Hwang et al 2017*, the experiment this project was directly following as well as based on.

Experimental Preparation of Animal Subjects

All animals used in the experiment were Black-6 mice with varying genotypes (retrograde tracing: wildtype C57BL/6J; calcium imaging: cross between *Rosa26-CAG-LSL-tdTomato,* Camk2a-tTA [JAX 003010], and tetO-GCaMP6s [JAX 024742] or cross between Camk2a-tTA [JAX 003010] and tetO-GCaMP6s [JAX 024742]; optogenetic perturbation: *Rosa26-CAG-LSL-tdTomato*), with both sexes represented.

Head-fixation plate/bar implantation

Surgical procedures were done a minimum of 8 weeks after birth. Animals were anesthetized with veterinary isofluorane, and betadine was used as a disinfectant on the scalp. The scalp was removed and the skull was scraped to remove the periosteum. Stereotaxic manipulation was used to produce a defined level plane with which skull markings were made. Acceptable margin of error was ± 20 µm superior/inferior from reference point (X-axis: 3000 microns from midline on right was compared to same position on left, Y-axis: bregma was compared to lambdoid suture). Bregma was defined as the intersection of the midline and

coronal suture as if it were was a straight line. An imaginary intersection was created to compensate for the inconsistency of true bregma between animals. The skull was marked at desired locations like the PPC, striatum (STR) and M2. A headbar or headplate was affixed to the skull with superglue and reinforced with dental cement leaving the areas of interest such as PPC, STR, and M2 uncovered. Once the superglue and dental cement were cured, we performed additional surgical procedures described in the next sections. After surgical completion animals were injected with baytril and buprenorphine subcutaneously and monitored until it was capable of walking on its own.

Surgical procedures for imaging experiment

After the headplate implantation, small craniotomies (bur holes) were made in the skull over the projection target area, STR or M2, to allow for insertion of a glass pipette loaded with retrograde Cre-encoding Canine Adenovirus (CAV-CRE). Pipettes were made with a tip diameter of 24-36 µm. The projection target areas were marked using their stereotaxic coordinates (STR, 2.2mm lateral, 0.8 mm posterior from bregma at a depth of 2.5mm from the dura surface; M2, 0.5 mm lateral, 0.3 mm anterior from bregma at a depth of 0.35 mm from the dura surface). Unilateral injections were made in the right hemisphere of the brain. For M2 projection mice, pipette was front-loaded with 40-150 nL of undiluted CAV-CRE virus and the virus was injected at a rate of 20 nL per minute and the left to settle for 5 minutes prior to retraction. For STR-projection mice, pipette was front-loaded with 100-150 nL of undiluted CAV-CRE virus and 10 nL of paraffin oil after to prevent leaking of virus in the cortex above the striatum during insertion. Virus was injected at a rate of 20 nL per minute and then left to settle for 20 minutes prior to retraction. Retraction was done at a rate of 50 microns per minute while

slowly injecting paraffin oil and waiting 2 minutes every 100 microns. The slow retraction and oil injection was to prevent backflow of the injected virus.

All animals, expect for three *Camk2a-tTA::tetO-GCaMP6s::Rosa-CAG-LSL-tdTomato* mice, were given an additional injection of virus encoding Cre-dependent tdTomato (50 nl undiluted AAV-2-CAG-FLEX-tdTomato; UPenn Vector Core) in the marked PPC of the right hemisphere at a depth of 350 μm to label projection neurons with a fluorescent protein .

Mice for imaging experiments received a second surgery once they reached an expert level of performance in the behavioral task. In the second surgery, a craniotomy was made over PPC on the right hemisphere marked previously during the first surgery, and the exposed cortex was covered with an optical window to visualize neurons during two-photon imaging.

Surgical procedures of optogenetic experiment

Following the procedures described for imaging experiments, we injected retrograde CAV-CRE in target areas, M2 or STR, bilaterally, after the headbar implantation. Then we performed craniotomies removing skull over PPC bilaterally, and injected virus to express either halorhodopsin (AAV-2-EF1a-DIO-eNpHR3.0-eYFP;N=2) or ArchT (AAV-2-flex-ArhT-GFP;N=12) selectively in projection neurons. halorhodopsin is a light-activated chloride pump, while ArchT is a light-activated proton pump, so both proteins suppress the activity of neurons when light-activated. Both these proteins were tagged with a fluorescent protein for analysis after data was collected. After the injections in PPC, the exposed cortex was covered with optical windows, allowing efficient light transmission for optogenetic experiments.

Behavioral Training

Two weeks after surgery animals began a water restriction regiment, slowly normalizing them to a 1 mL per day regiment. Once their weight stabilized above 80% original body weight, behavioral training of a joystick task was started. The task was to press a joystick with their left paw in the correct direction indicated by a visual stimulus within a response period while an audio cue (go cue) was played to receive a water reward (Figure 1A).

Behavioral training was done in a blacked out behavioral box (40 cm x 40 cm x 40 cm) where a joystick was mounted to a platform with a detachable magnetic stage to hold the mouse. A computer monitor was used to display visual stimulus and a water port with infrared light emitting diodes to monitor licking. Visual stimulus displayed moving gratings in the direction of the desired target region. A stock joystick was used with 1/16 inch brass bar attached to be manipulated by the animals. An electromagnet was used to fixate the joystick to an origin position and would be used in tandem with a spring to return the joystick to origin position after each lever press. The joystick moved in a 2D space, and the two target zones were placed in two orthogonal directions (forward or downward; Figure 1B).

After successful trials, the target direction would either swap or remain the same up to a set maximum number of repetitions. Error trials were cued using a white noise auditory stimulus and water being withheld. After each error trial, the target direction was repeated until the zone was successfully reached as to prevent the animal from only learning to push the joystick in one direction.

Animals were weighed before and after each session to determine how much water was consumed, ensuring a minimum of 1 mL of water per day for each animal. Animals were trained

over the course of 2-4 months, during which the task was shaped to perform the memory-guided two-choice task described below, through multiple training steps similar to the procedures described in Hwang et al. Initial training was started with no discrimination -the trial would not be considered an error trial if the lever entered the alternative target zone before entering the correct target zone- and a 4 mm target distance within a 30 second response period. At each stage, a mouse that successfully completed the task with an 80% accuracy or higher would advance to the next stage. First, the response period was reduced to 10 seconds, and distance increased to 6 mm. The mouse then needed to discriminate between one of two directions to gain the reward; If the animal entered the alternative target area before the correct target area, the trial would be considered an error trial. Time between trials was increased prior to advancement to memory task, up to a 4 second inter-trial-interval. In the memory task, the visual stimulus was turned off prior to the response period. Time between the removal of the visual stimulus and the onset of the response period (i.e., delay period) increased until reaching the final stage of training. Expert mice were defined as animals who could correctly remember and press the lever in the direction shown by a 1 second visual stimulus after a 2 second delay period and within a 10 second response period for at least 60% of trials. Each session ended either at 170 successful trials or after an hour within the behavioral rig, whichever came first. Water rewards should have provided roughly 1 mL of water if the mouse completed the 170 successful trials, extra was administered to meet the 1 mL per day requirement if they had not received it during the session.

Two-photon Calcium imaging and Analysis

Expert mice that performed the memory task with performance above 60% were allowed full water access for a few days prior to a second surgical procedure described. After a recovery from the second surgery and water restriction period, mice resumed training in a behavioral rig

containing a two-photon microscope and acclimated to the new environment for a few days before imaging.

The microscope functioned with a water immersion lens, so water was added on top of the window to produce clear images in each session. A blackout shroud was used to prevent a light artifact from the monitor displaying visual stimulus during imaging. Each mouse was imaged for approximately 11 days, each day collecting data from different fields in PPC. The lens was capable of collecting fields of approximately 500 µm x 500 µm. Each imaging field was in layer 2/3, approximately 250 to 350 µm below the surface of the cortex.

Single cell activity:

Using custom MATLAB program, fluorescence images were aligned frame by frame to compensate for lateral motions of the brain during imaging. Regions of interest (ROIs) were manually drawn on the motion-corrected fluorescence images, by circumscribing the cell bodies based on their GCaMP fluorescence intensity distinguishable from the background. Pixels inside each ROI were considered as a single cell, whereas pixels extending radially outward from the cell boundary by 2-6 pixels were considered background. In cases where the background included other cells' ROIs, those pixels were excluded. To estimate the activity of a single cell, 70% of the average pixel intensity in its background was subtracted from the average pixel intensity inside the cell. The time series of the background-adjusted intensity was transformed to dF/F by dynamically estimating the baseline intensity (i.e., the 8th percentile of the intensity distribution in the 20 second window centered at each time point). dF/F was further transformed into an estimate of spike rates using the spike-triggered mixture model (https://github.com/lucastheis/ c2s).

Choice selectivity during the ITI:

For each neuron, choice selectivity was examined during the ITI. We performed receiver operating characteristic (ROC) analysis on the time-averaged activity during the ITI, using the binary choice as label and the activity as score. For a significance test, we used the 99.9th percentile of the null distribution of selectivity strength estimated by choice label shuffling per cell and epoch, 1000 times.

Optogenetic Inactivation

Bifurcated optic fibers were connected to a laser with a wavelength of 532 nm at ~28mW power between the fibers and placed over either the craniotomy window (experimental) or the animal's neck (control) during behavioral sessions. Windows were cleaned before each inactivation session. Fibers were ~4mm apart and placed close to the window without touching it. Placement of the fiber over the window was supposed to be in the center of the expression, so expression levels and location were visually confirmed prior to beginning the inactivation sessions.

For both experimental and control sessions the laser was on once between at least 5 light off trials and only during the ITI. This came out to be roughly 15% of all trials were "Laser On" while the remainder were "Laser Off". A total of 5 inactivation days and control days were each recorded, oscillating between control and inactivation days. Any day which the experimental apparatus malfunctioned, the animal completed less than 100 successful (non-error) trials, and/or had a performance not significantly higher than chance were excluded from the data sets analyzed.

Behavioral modeling

The same behavioral model was used to analyze this set of mice as those from the *Hwang et al 2017* paper. The model was designed to weigh the sum of the previous trial choices the animal had made, the outcomes of the previous trials, the interaction between these variables, and a constant: it used this information to predict the choice behavior of the animal in the current trial (Equation 1). Prior trials were weighed with an exponential decay of their value as its distance from current trial increased. The choice and outcome were all given a value of either 1 or -1. In instances where the animal did not move the joystick the choice value was 0 and the outcome was 1, which is defined as an error.

$$\log \frac{probability\{choice(N) = forward\}}{probability\{choice(N) = downward\}} = w_o \cdot \sum_{k=1}^{N-1} outcome(k) \cdot e^{-\frac{N-1-k}{\tau_o}} + w_c \cdot \sum_{k=1}^{N-1} choice(k) \cdot e^{-\frac{N-1-k}{\tau_c}} + w_{oc} \cdot \sum_{k=1}^{N-1} outcome(k) \cdot choice(k) \cdot e^{-\frac{N-1-k}{\tau_{oc}}} + constant$$

We used 10-fold cross validation to measure accuracy of models. To do this, the data set was divided into 10 non-overlapping portions, with one part was defined as the test set and compared to the other 9 portions, defined as training sets. After this a second set was defined as the test set and the other 9 were training, with this repeating until each of the 10 parts were individually compared to the other 9 parts. The model's accuracy was measured by taking the fraction of the models estimated choice of the animal against the animal's actual choice.

Histology

Some animals were perfused with 4% PFA and had the brain extracted. Brains sat in PFA for 1-2 days before they were transferred to 30% sucrose. Once the tissue had sunk to the bottom of the liquid, the brain was cut using a microtome into 60 µm slices. Some brains were simply mounted to glass slides with CC/mount, while others were stained using NeuN primary antibodies and one of three antibodies tagged with a fluorescent protein of 350nm, 488nm or 568nm wavelength prior to mounting.

Stained slices were used to count the number of cells which had been infected via the CRE and Halo/ArchT injections and compared to the total number of neurons in the region. NeuN was used as opposed to DAPI staining to prevent the counting of non-nerve cells like glial cells: NeuN being a nuclear bound protein specific to neurons, so only those cells would be tagged (Gusel'nikova & Korzhevskiy, 2015). The staining solutions used were a 1:400 concentration of primary mouse-anti-NeuN antibody to blocking solution, and a 1:1000 concentration of secondary goat-anti-mouse antibody with one of three fluorescent tags. Blocking solution was made with 30ml of 1x PBS, 0.3g of BSA, 0.6ml of NGS and 900 µl of 10x Triton. Slices were incubated in blocking solution for 1 hour at room temperature before being transferred to the primary antibody solution to incubate overnight at 4°C on a rocker. The slices were then washed in PBS 4 times on a rocker for 20 minutes at room temperature, followed by a 2-hour incubation in the secondary antibody at room temperature. The slices were washed again and then mounted using CC/Mount.

The whole slice was photographed using an Axio-Zoom microscope. Marking were made on the photos at 1700 µm from the midline, this point defined the center of the PPC. Photos were taken through a 20x lens to create a 600 µm wide plane that extends from the bottom of the

cortex, marked by the corpus collosum, to the top of the cortex. Planes were photographed from 300 µm anterior to 300 µm posterior to the center of the PPC. Within this region, projection cells were counted and in comparison, to the NeuN stained cells within that region to quantify the percentage of cells that are projecting to the striatum and will be inactivated during the optogenetic experiments.

Monosynaptic Rabies Projection Labeling

A small set of mice (N=10) were injected with CAV-CRE in either the striatum or M2 in the right hemisphere following the procedures described above, and 200 nL of AAV-EF1a-DIO-mRuby2-P2A-TVA in PPC. After allowing for 3 weeks of expression, 150 nL of AAV-EF1a-DIO-RVG was injected in PPC. The viral concentration was high enough to where it could jump synapses once to cells that project to and from PPC. After a week, the animals were perfused and the brains extracted. The brains were soaked in PFA and transferred to sucrose to soak for a total of 4 days, 2 days each. The brains were sliced, each section being 60 µm in thickness. The slices were stained with DAPI and mounted before being photographed and analyzed.

Utilizing a mouse brain atlas[20] each slice with green labeled (rabies infected) cell somas were mapped to various regions of the brain. Once each rabies infected cell was counted and sorted, the data was normalized to the percentage of cells in a particular region to the total number of cells in the brain (i.e. M2, M1, V2MM, lPtA, etc.). Only regions that possessed more than 1% of the total cells were included in the analysis.

Results

Choice Tuning of Projection Neurons

We first confirmed that the posterior parietal cortex (PPC) projects to the dorsal striatum (STR) and the posterior secondary motor cortex (M2), by examining the retrograde labelling in PPC after injecting the retrograde Cre-encoding CAV virus (CAV-CRE) in STR and M2 in separate mice (Figure 1C-E). To study the activity of the labelled projection neurons through two-photon calcium imaging, we applied the same retrograde labelling in transgenic mice (CaMK2-tTA::tetO-GCaMP6s or CaMK2-tTA::tetO-GCaMP6s::Rosa-CAG-LSL-tdTom) in which excitatory neurons express GCaMP6s (Figure 1E). We found that the STR projection cells were found much deeper in the PPC than the M2 projection cells (Figure 1H). M2 projection cells were more likely to be found around 250μm from the surface of the cortex, while striatal projection cells were found on average at 350μm from the surface. When comparing these two groups, we saw that the number of co-labeled cells were not significantly different: Co-labeling was found by dividing the number of cells with both red and green fluorescent expression by the number of red-labeled cells (Figure 1I). This shows that the expression of GCaMP6S is not different between the two groups. The number of projection neurons, however, was seen to be significantly different between the two projection groups, with the PPC containing significantly more cells that project to the striatum than those that project to M2 (Figure 1J). The number of projection neurons was determined by dividing the number of cells labeled both red and green by the total number of cells that had the green label. These differences in depth as well as gross number of projection cells can be seen in the histological data in Figure 1D, as well as the two-photon calcium imaging, represented in Figure 1E.

To compare the functional properties of the two projection groups, we analyzed the activity of the projection neurons while mice performed the memory-guided two-choice task. Previously, Hwang et al., showed that PPC neurons encode the upcoming choice information during the inter-trial interval (ITI) prior to the presentation of the task-relevant stimulus, and related the ITI activity to the history-based bias. Consistent with Hwang et al., we found PPC neurons are tuned to the upcoming choice but the two projection groups showed different prevalence in tuning. We saw that during the ITI, the STR projection neurons had a much higher percentage of cells tuned to the upcoming choice than those of the non-labelled neurons, while M2 projection cells had a significantly lower percentage of tuning than their non-labelled counterparts (Figure 1F). As a result, STR projection neurons are significantly more likely to encode the upcoming choice information during the ITI than M2 projection neurons or non-labelled neurons (Figure 1G). This result suggests that PPC might transmit the history-based choice bias preferentially to STR.

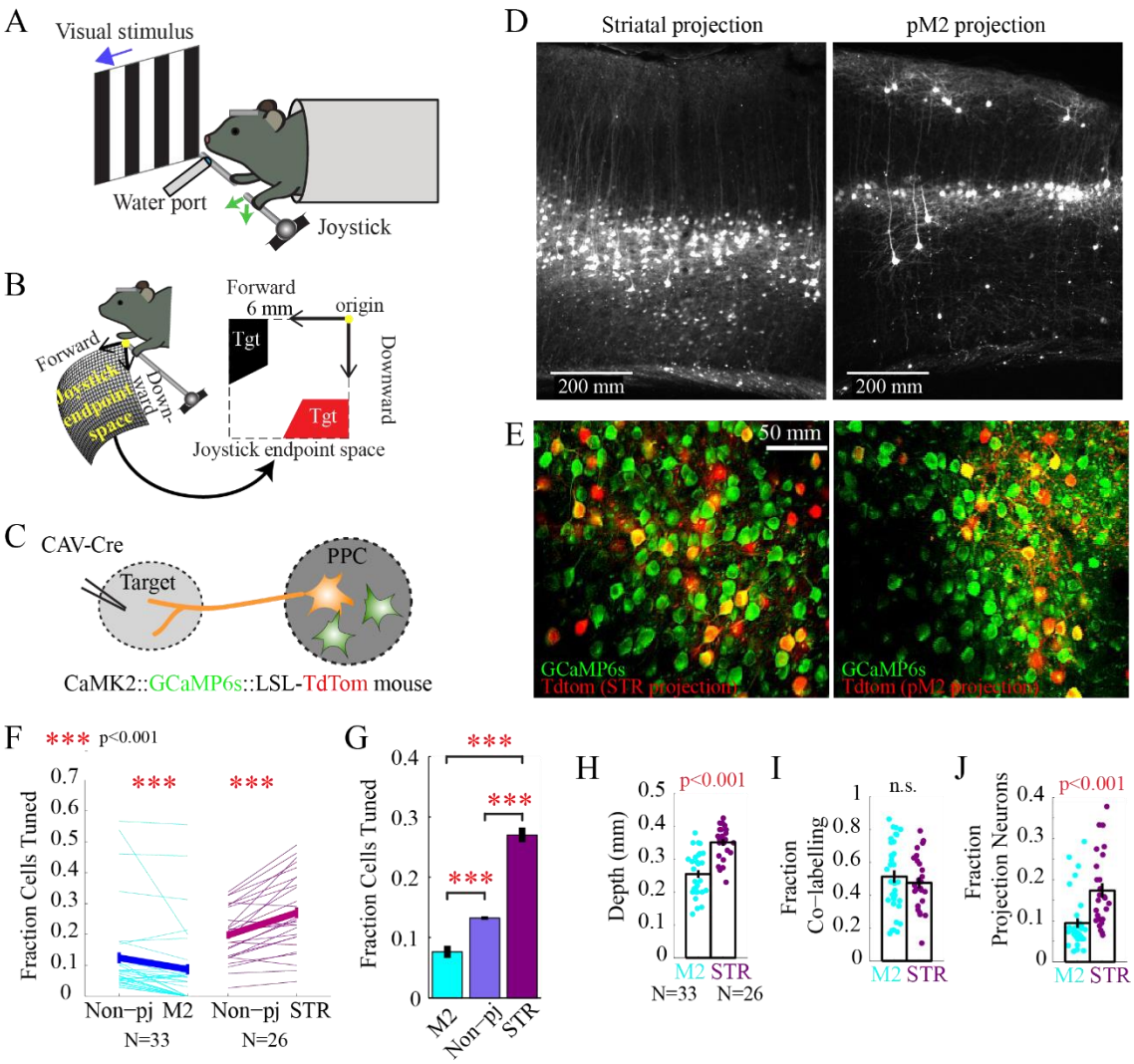

Figure 1: Two-photon calcium imaging of projection neurons from either STR or M2. A) Schematic of the behavioral task. B) Schematic of the task target space, with 2 possible target zones, forward and downward. C) CAV-Cre is injected into either the STR or M2 of a CamK2::GCaMP6S::LSL-tdTomato mouse. All animals used in two-photon calcium imaging had this genotype, as well as those used for section (D). D) Histological data from two different animals, one with an injection into the STR (left) and M2 (right). E) Two-photon calcium microscopy images, with STR (left) and M2 (right) cells labeled with CAV-Cre dependent tdTomato proteins. F) Graphical comparison of the tuning of active cells, comparing M2 projection cells to non-projection, and STR projection cells to non-projection cells (M2/non p<02e-4, STR/non p<6e-5). G) Bar Graph comparing the fraction of cells tuned to the task between M2, non-projection cells, and STR projection cells. H) Comparing the difference in depth of M2 projection and STR projection cells. I) Comparing the average number of red+green cells in M2 and STR based on the number of red cells. J) Comparing the number of red+green cells in M2 and STR based on the number of green cells.

Graph 1: The fraction of cells tuned to a specific time-based variable or combination of variables. The variables are based on Equation 2. Significance was based on the fraction of cells that have a variable weight significantly higher than 0.

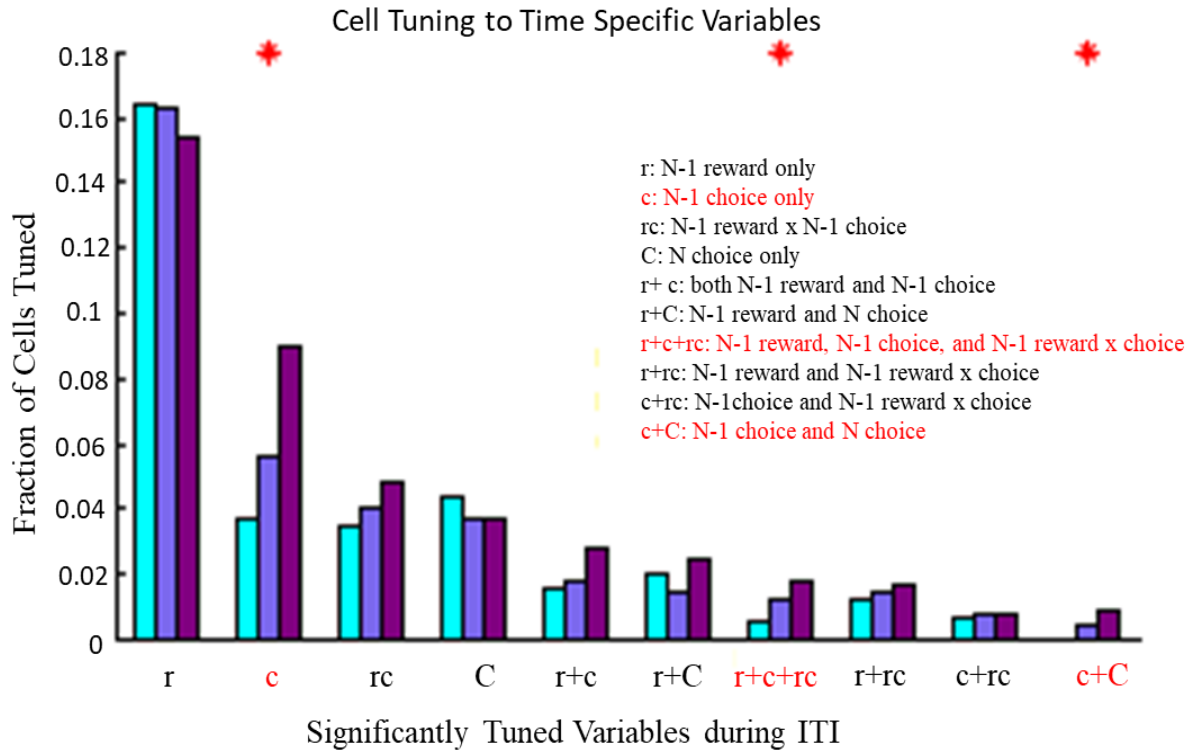

The upcoming choice is highly correlated with the history-based internal bias, thus it is possible that individual neurons encoding history information could appear to be encoding the upcoming choice. To disambiguate the information coding by individual neurons, we applied a multiple linear regression on the ITI activity and determined which variables significantly modulated the activity (Equation 2).

$$ITI\ activity\ of\ neuron\ (N)$$
$$= w \cdot choice(N) + w_o \cdot outcome(N-1) + w_c \cdot choice(N-1) + w_{oc}$$
$$\cdot outcome(N-1) \cdot choice(N-1)$$

We see significant differences in encoding 3 variables in Graph 1. The STR projection group shows a significantly higher fraction of cells with a significant weight for the N-1 choice, the N-1 reward & N-1 choice & N-1 reward x choice complex, and the N-1 choice & N choice combination variables than the M2 projection group. The STR projection cells are more prevalently tuned to variables including the choice made in the previous trial. This strongly indicates that the previous choice history information is preferentially encoded in the STR projection cells.

Taken together, we saw that not only were there more total cells projecting to STR than M2, but there were significantly more prevalent internal bias coding in STR than M2. This suggests that the STR projection neurons were responsible for the production of the history-based bias seen in the Hwang et al, 2017 paper.

Striatal projection inactivation alters history-based choice bias

We hypothesized, based on previous information pertaining to PPC projections, that projection cells terminating in the striatum were be responsible for the changes in the history-based bias when the entirety of the PPC was inactivated, seen in the previous experiment published (Hwang et al, 2017). To test this, we expressed eNpHR3.0 or ArchT selectively in projection cells (Figure 2A) and trained mice in a joystick task to remember the direction of a visual stimulus after a short delay to receive a reward, the same as those animals imaged under the two-photon microscope. A bifurcated optic fiber was placed over one of two locations, either the bilateral windows over the PPC, or over the headbar/neck of the animal in alternating

sessions (Figure 2B). The power output of the laser checked before inactivation sessions was between 20 and 40 mW.

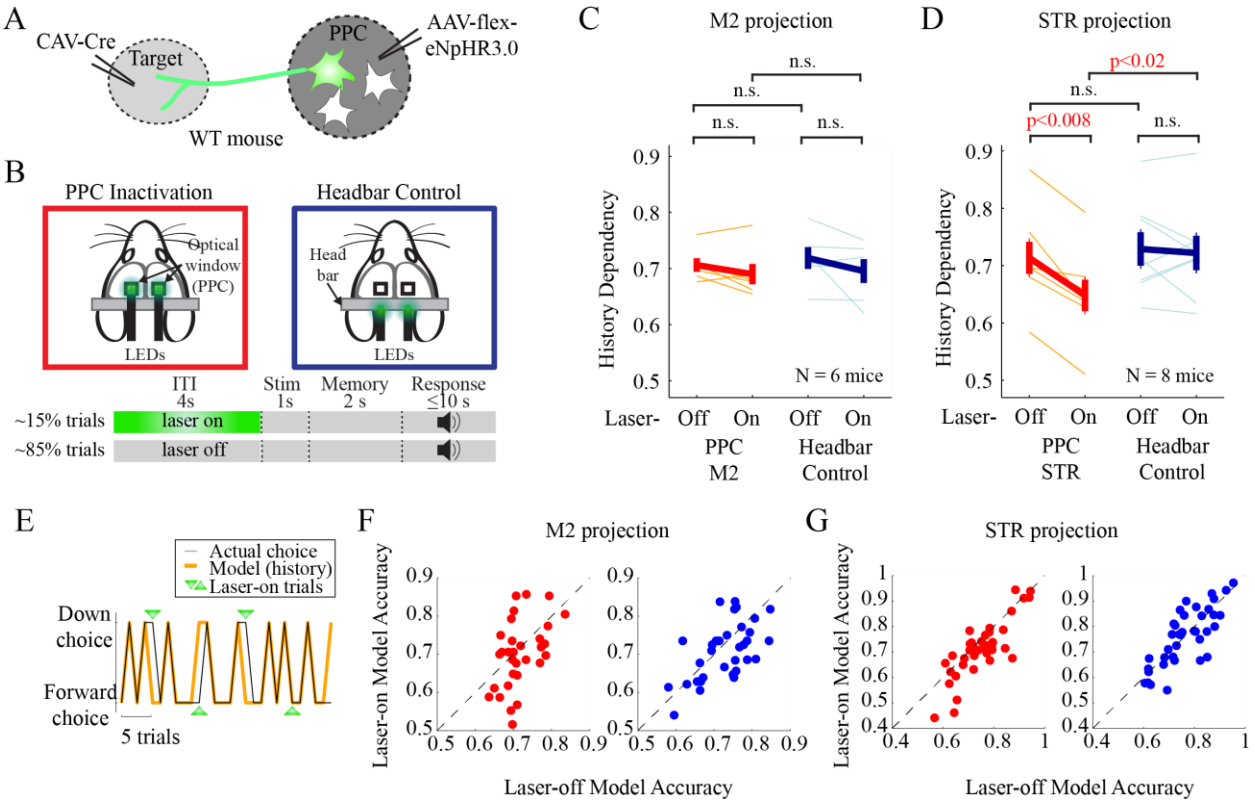

Figure 2: Analysis of optogenetically inhibited projection neurons within the PPC. A) Schematic of the injection methodology. Animals had either a WT or tom +/+ genotype B) Schematic of what was considered control and inactivation trials. The laser was turned on during the ITI for all but a small subset of mice, which after ITI inactivation experimentation underwent Trial inactivation sessions, in which the laser was on during all times outside of the ITI at the same frequency as ITI inactivation (not shown). C,D) Comparing the accuracy of the behavioral model during inactivation and control sessions when the laser is off and on. C) M2 projection ITI inactivation and control sessions. D) STR-projection ITI inactivation and control sessions. E) Visual representation of behavioral model. The black line shows the actual choice of the animal, while the solid orange line was the model's prediction. Green arrows indicated trials in which the laser was turned on and the PPC was inactivated. F,G) Linear regression of laser sessions, comparing the accuracy of the behavioral model when the laser is on and when it is off during F) M2-projection ITI and G) STR-projection ITI trial inactivation and control sessions.

We performed inactivation experiments on STR projection neurons in 8 mice, and M2 projection neurons in 6 mice. The behavioral data was analyzed using a model (Equation 1), which was constructed to predict the choice of the animal based only on the session history. The model was built from laser light-off trials and applied to a separate set of light-off or light-on test

trials. If the model's accuracy were to decrease only during test trials in which the laser was turned on in the inactivation but not control sessions, the change in accuracy would be a direct result of the inactivation of the projection cells within the brain.

We utilized the logistic regression model described in the methods, which uses choice-outcome information of previous trials to predict the choice of the animal in the current trial (Equation 1). We had found that across animals there was a roughly 70% accuracy of the model when the laser was turned off (Figure 2C and 2D). We saw no significant difference between the model accuracy in predicting the animal's behavior during Light over Headbar when comparing light off to light on trials in both STR projection and M2 projection groups.

We found no significant difference between the accuracy of the behavioral model when comparing the light on to light off trials during M2 inactivation sessions, as well as comparing the difference between light on during inactivation sessions and light on during control sessions (Figure 2C). This trend is also seen in the session-to-session analysis, which shows that data do not shift significantly from the unity line (Figure 2F).

Comparing this data to that of STR projection cells, we saw a significant difference between the light on and light off trials when the optic fibers were placed over the PPC during the inactivation trials ($p<0.008$) (Figure 2D and 2E). The Light on trials during inactivation sessions significantly decreased the accuracy of the model when comparing them to light off trials, as well as light on trials during control sessions. Individual sessions also show this change in accuracy (Figure 2G). The decrease in the model's ability to predict choice shows that the history-dependency was being altered. This suggests that the STR projection neurons within the PPC are responsible for the production of history-dependent choice bias.

Monosynaptic Rabies Tracing of Projection neurons

The results thus far suggest that history-based choice bias is preferentially controlled by the STR projection cells in PPC instead of M2 projection cells. The difference raises the possibility that the two projection groups might receive different input information from the upstream areas. To test this possibility, we examined the input connectivity of the projection neurons using a monosynaptic rabies-virus tracing. A group of mice were given unilateral CAV-CRE injections into the right-side of either the STR or M2, and AAV-EF1a-DIO-mRuby2-P2A-TVA in PPC, and then EnvA-RVdG-GFP in PPC to allow the Glycoprotein depleted Rabies virus to jump a single synapse and infect an adjacent synapsed neuron (Osakada et al, 2013)(Callaway et al, 2015). This allows us to trace the connections from the neurons projecting to either STR or M2 and see what other regions are feeding information to these cells. We traced and counted the numbers of labeled cells in the two projection groups of mice (N = 2 per group). We utilized the Mouse Brain Atlas to map the green-labeled cells into the various regions of the brain. Cells within a specific region of the brain in the same hemisphere as the CAV-CRE injection site were counted and normalized to the percentage of the total cells in the hemisphere.

We found that within the STR projection traces, a large percentage of cells were counted within the barrel field of the primary somatosensory cortex, as well as traces in V1, V2L and V2M (Graph 2). This is consistent with previous information, which showed input connections to PPC (Hovde et al, 2018). However, unlike the STR projection traces, we did not see consistent connections among the M2 projection brains thus far. Some regions, such as S1FL and V1 had a high percentage of cells in one brain, while having next to none in the other traced brain. More data is required to make any definitive statements about the connections of either group of projection neurons. The standard deviation of each of the brains was too great to make any

claims in regard to the distribution of neurons that synapse with PPC projection cells. Because of this high standard deviation, we did not see significant differences between the traces of M2 and STR projection cells.

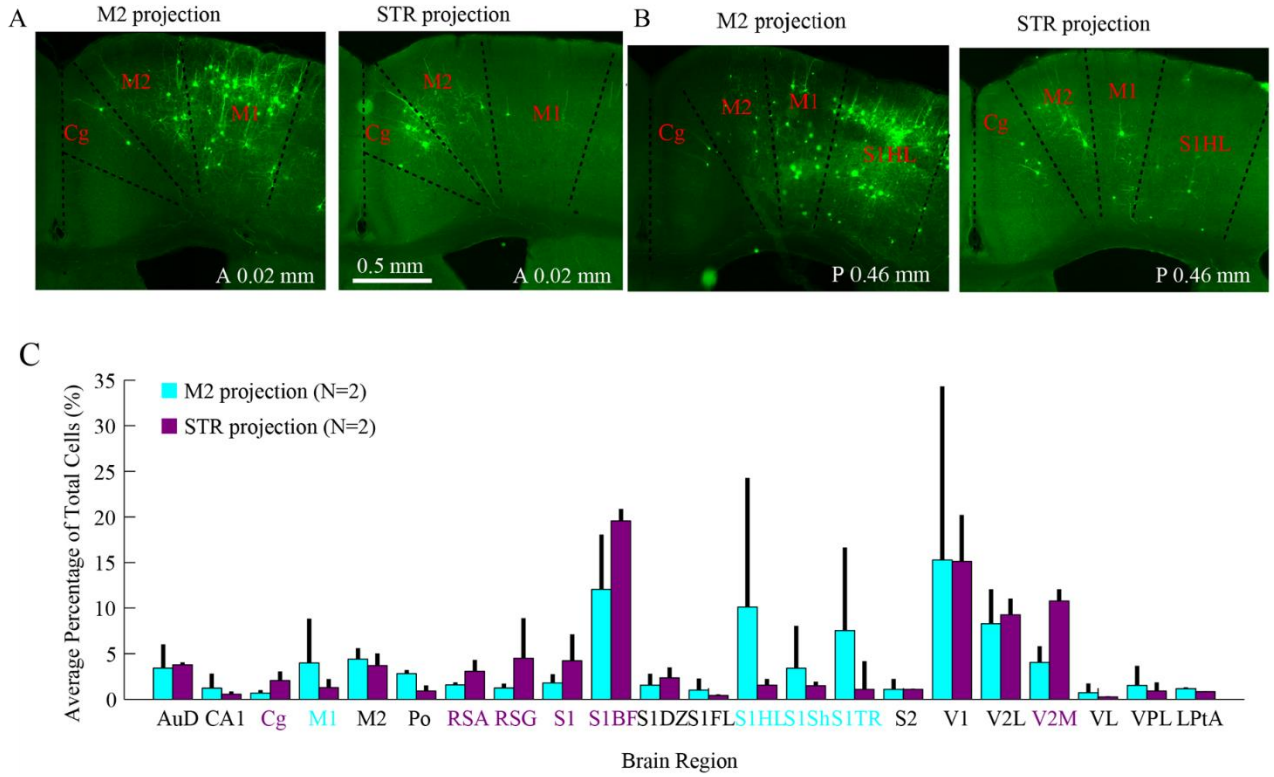

Figure 3: A&B) Histological data displaying the differences of Rabies traced brains, particularly those of the cingulate cortex, M1 and S1HL. C)Graphical representation of cells which synapse to either STR or M2 projection cells in the PPC. M2 and STR projection groups normalized number of cells in each region to percentage of total cells, and then averaged between similar STR or M2 projection cells. Standard deviation represented by error bars. Regions were defined as significant if they contained greater than 1% of the total traced cells.

Nevertheless, we see some differences in regions such as the Cingulate cortex and primary motor cortex. M1 and S1HL are shown to have substantially higher fractions of cells projecting to M2 than that of STR (Figure 3B). Conversely, we saw a substantial number of cells

traced to the cingulate cortex - areas 1 and 2 were treated as a single region- from STR projection cells, which was absent in brains traced from M2 projection cells (Figure 3A). A similar trend is seen in the retrosplenial cortex, where both the granular and agranular regions had a higher average percentage of cells traced from STR projection neurons. Overall, we can see that there is a trend of inputs coming from the association areas and terminating on STR projection cells in PPC, while sensorimotor regions synapse with M2 projection cells. Although more data is necessary to be conclusive, STR projection and M2 projection cells are very likely to receive different input from associative and sensory cortices, underlying different information processing between the two groups.

Discussion

Across our data, we found the striatal projection cells being more significantly implicated in history-dependent behavior than that of projection neurons to M2. Firstly, we found that STR projection neurons are encoding history-dependent choice information at a higher fraction than that of M2 projection cells, shown through two-photon imaging experiments. Secondly, we found that STR projection neurons, unlike M2 projection neurons, are responsible for the bias information, shown in the optogenetic experiments. Finally, we saw trends suggesting differences in the inputs of these two groups of projection cells. The combination of data from the two-photon calcium imaging as well as the optogenetic data provides a good amount of evidence in favor of the hypothesis of history-dependent choice information being offloaded to the striatum. This compounded with consistencies between this project and the previous Hwang et al, 2017 paper, showing that the information is being transferred prior to the onset of the visual stimulus, leads to the conclusion that striatal projection cells are responsible for the production and transfer of history-based bias.

While we were able to conclude this, there are some stipulations that much be added to this claim. Currently, the number of M2 projection mice is not equal to that of the striatal projection mice used in the data set (N=6 vs N=8). This is purely due to time constraints. The average time it takes for animals to be trained is roughly 2 months, and not every animal makes it to the expert stages of the experiment. Among those that do, some are unable to be used for data collection for a few reasons. For instance, some animals did not express halorhodopsin or ArchT bilaterally, and had to be removed from the pool of potential test animals. Others were able to learn the task and become experts, but once the laser was introduced the animal was no longer able to complete the task. Those animals attempted to be retrained, but this added significantly more time. Some others were unable to complete the task with a performance significantly higher than 50%, and we had to remove them from the experimental pool. This combined with the of the number of behavioral boxes (three) we possessed, the number of animals that could be trained simultaneously was limited.

This time limitation was also a problem when it came to the production of rabies tracing brains. Given more time to prepare and complete more rabies tracing analysis, they would be more complete, and provide more statistical weight. Based on the current trends in the data, we can presume that these would hold if more data was gathered.

All of the cells inactivated in the PPC were somas of the neurons, limiting the evidence to the activity of the cell bodies themselves. It is well known that the axons of neurons can project to multiple targets. While we now know the neural somas projecting from PPC to STR encode bias information, we do not know if the final destination of the information is the striatum. The cells could be relaying the information to another region of the brain, such as the thalamus or superior colliculus, and these cells are simply projecting collaterally to both that and the striatum.

We need to do terminal inactivation experiments to prove the information is being sent to the striatum. It is possible that the bias information is being transmitted to another region, like the thalamus, and because some striatal projection cells terminate in both the striatum and thalamus, we may be falsely equating bias information with this set of neurons.

Additionally, we do not know if striatal projection neurons are sufficient for encoding the bias information. It is possible that these cells are not the only ones that are responsible for the integration of the history-dependent information, and others are required. As previously stated, we had only looked at the cells projecting to the striatum and secondary motor cortex, and the PPC does have a variety of inputs and outputs. The information could in fact be going to both the striatum and thalamus, with both inputs being required for the integration of bias information into behavioral changes.

Conclusion

Our results have been shown to be consistent with previous data known about not only the functions of the PPC and striatum, but also consistent with the results found in the previous Hwang et al, 2017 paper. It can be stated that with the evidence gathered from the two-photon imaging and the optogenetic experimentation that the striatal projection neurons are responsible for the production of history-based behavioral bias in mice. Additionally, while no significant differences are seen from the Rabies tracing data, trends can be seen to suggest differences in the inputs of those projection cells.

This thesis is in part currently being prepared for submission for publication of the material. Hwang, EunJung; Link, Trevor; Lu, Shan; Komiyama, Takaki. The thesis author was a primary investigator of this material.

References

1) Balleine, B. W., Delgado, M. R., & Hikosaka, O. (2007). The Role of the Dorsal Striatum in Reward and Decision-Making. *Journal of Neuroscience,27*(31), 8161-8165. doi:10.1523/jneurosci.1554-07.2007

2) Erlich, J. C., Brunton, B. W., Duan, C. A., Hanks, T. D., & Brody, C. D. (2015). Distinct effects of prefrontal and parietal cortex inactivations on an accumulation of evidence task in the rat. *ELife,4*. doi:10.7554/elife.05457

3) Goard, M. J., Pho, G. N., Woodson, J., & Sur, M. (2016). Distinct roles of visual, parietal, and frontal motor cortices in memory-guided sensorimotor decisions. *ELife,5*. doi:10.7554/elife.13764

4) Goldberg, J., & Reynolds, J. (2011). Spontaneous firing and evoked pauses in the tonically active cholinergic interneurons of the striatum. *Neuroscience,198*, 27-43. doi:10.1016/j.neuroscience.2011.08.067

5) Gremel, C. M., & Costa, R. M. (2013). Premotor cortex is critical for goal-directed actions. *Frontiers in Computational Neuroscience,7*. doi:10.3389/fncom.2013.0011

6) Gusel'nikova, V. V., & Korzhevskiy, D. E. (2015). NeuN As a Neuronal Nuclear Antigen and Neuron Differentiation Marker. *Acta Naturae, 7*(2), 42–47.

7) Harvey, C. D., Coen, P., & Tank, D. W. (2012). Choice-specific sequences in parietal cortex during a virtual-navigation decision task. *Nature,484*(7392), 62-68. doi:10.1038/nature10918

8) Hovde, K., Gianatti, M., Witter, M. P., & Whitlock, J. R. (2018). Architecture and organization of mouse posterior parietal cortex relative to extrastriate areas. doi:10.1101/361832

9) Hwang, E. J., & Andersen, R. A. (2011). Effects of visual stimulation on LFPs, spikes, and LFP-spike relations in PRR. *Journal of Neurophysiology,105*(4), 1850-1860. doi:10.1152/jn.00802.2010

10) Hwang, E. J., Dahlen, J. E., Mukundan, M., & Komiyama, T. (2017). History-based action selection bias in posterior parietal cortex. *Nature Communications,8*(1). doi:10.1038/s41467-017-01356-z

11) Mohan, H., Haan, R. D., Mansvelder, H. D., & Kock, C. P. (2018). The Posterior Parietal Cortex as Integrative Hub for Whisker Sensorimotor Information. *Neuroscience,368*, 240-245. doi:10.1016/j.neuroscience.2017.06.020

12) Morcos, A. S., & Harvey, C. D. (2016). History-dependent variability in population dynamics during evidence accumulation in cortex. *Nature Neuroscience,19*(12), 1672-1681. doi:10.1038/nn.4403

13) Nachev, P., Kennard, C., & Husain, M. (2008). Functional role of the supplementary and pre-supplementary motor areas. *Nature Reviews Neuroscience,9*(11), 856-869. doi:10.1038/nrn2478

14) Parker, N. F., Cameron, C. M., Taliaferro, J. P., Lee, J., Choi, J. Y., Davidson, T. J., Daw, N. D., Witten, I. B. (2016). Reward and choice encoding in terminals of midbrain dopamine neurons depends on striatal target. *Nature Neuroscience,19*(6), 845-854. doi:10.1038/nn.4287

15) Paxinos, G., & Franklin, K. B. (2004). *The mouse brain in stereotaxic coordinates*. San Diego: Academic Press.

16) Stocco, A., Lebiere, C., & Anderson, J. R. (2010). Conditional routing of information to the cortex: A model of the basal ganglia's role in cognitive coordination. *Psychological Review,117*(2), 541-574. doi:10.1037/a0019077

17) Sugrue, L. P. (2004). Matching Behavior and the Representation of Value in the Parietal Cortex. *Science,304*(5678), 1782-1787. doi:10.1126/science.1094765

18) Tepper, J. M., Tecuapetla, F., Koós, T., & Ibáñez-Sandoval, O. (2010). Heterogeneity and Diversity of Striatal GABAergic Interneurons. *Frontiers in Neuroanatomy,4*. doi:10.3389/fnana.2010.00150

19) Yager, L., Garcia, A., Wunsch, A., & Ferguson, S. (2015). The ins and outs of the striatum: Role in drug addiction. *Neuroscience,301,* 529-541. doi:10.1016/j.neuroscience.2015.06.033

20) Znamenskiy, P., & Zador, A. M. (2013). Corticostriatal neurons in auditory cortex drive decisions during auditory discrimination. *Nature,497*(7450), 482-485. doi:10.1038/nature12077